Technical Document 2892
February 1996

Spectral Correlation Properties of Time Series Due To An Acoustic Source Moving Through An Oceanic Waveguide

M. Reuter

EXECUTIVE SUMMARY

The time series representing the acoustic energy received at two sensors due to a source moving through an oceanic waveguide can exhibit strong spectral correlation between different frequencies. This correlation can be exploited to enhance passive detection of moving targets—particularly in shallow water and near-field environments.

The structure of this spectral correlation is derived in this document. It is also shown that established techniques can estimate the spectral correlation from time series. This algorithm is assessed on real underwater acoustic data. Excellent agreement is observed with theory.

CONTENTS

Appendices

Figures

1. INTRODUCTION

Many algorithms used in SONAR signal processing require the estimation of auto- and cross-spectra of time series received at an array of sensors. A fundamental assumption is that the time series is stationary. However, a moving source destroys stationarity between sensors. This is quite problematic for the estimation of second-order moments. In practice, one assumes that the data are piecewise stationary, i.e., that the moments can be estimated from sufficiently long segments of data. This assumption may not be valid for sources in a near-field or shallow-water environment.

In this document, we define and derive the 2-D spectrum of a broadband source moving through an oceanic waveguide. We show how an established technique exploits the structure of the 2-D spectrum to estimate a related quantity, the 2-D spectral coherence. This technique accounts for source motion in the spectral analysis algorithm by using the spectral correlation properties of non-stationary processes. By incorporating this spectral analysis approach, the detection performance of signal and array processing algorithms is enhanced since the 2-D spectral coherence can be used as a discriminant for moving targets.

In section 2, we derive the 2-D spectrum for an acoustic source moving through an oceanic waveguide and describe the algorithm that estimates the 2-D spectral coherence from time series. In section 3, we move from this theory to the real world. We analyze experimental data and compare these results to the theory. Section 4 contains a summary and in section 5 we recommend several ways to exploit these results.

2. 2-D SPECTRUM OF A MOVING SOURCE

Hawker (1979) originally derived the pressure field generated by an acoustic source moving through an oceanic waveguide. We related Hawker's results to time-varying linear system theory and used them as a basis for an acoustic time series simulation (Reuter, 1994). In this section, we briefly review these results. We then derive the 2-D spectrum (Hurd, 1989) of an acoustic source moving through a waveguide and describe an algorithm that generates a consistent estimate of the 2-D spectral coherence (Hurd & Gerr, 1991).

2.1 2-D SPECTRUM IN TIME-VARYING LINEAR SYSTEMS

The impulse response and the bifrequency system function $\Gamma(\omega, u)$ of a time-varying linear system are related by the Fourier transform pair (Reuter, 1994; Zadeh, 1950)

$$h(t, -\tau) \overset{\mathcal{F}}{\Leftrightarrow} \Gamma(\omega, u). \tag{1}$$

If $\{y_1(t)\}$ and $\{y_2(t)\}$ are the outputs of two real, stable linear systems driven by the same real, wide sense stationary process $\{x(t)\}$, then the 2-D spectrum between $\{y_1(t)\}$ and $\{y_2(t)\}$ is given by Reuter (1994)

$$S_{12}(\alpha,\beta) = \frac{1}{2\pi}\int S_x(\omega)\Gamma_1(\omega,\alpha)\Gamma_2^*(\omega,\beta)d\omega, \tag{2}$$

where $S_x(\omega)$ is the power spectral density of the process $\{x(t)\}$. $S_{12}(\alpha,\beta)$ describes the joint spectral correlation property of processes $\{y_1(t)\}$ and $\{y_2(t)\}$.

If the linear systems were also time invariant, the 2-D spectrum can be shown to be (Reuter, 1994)

$$S_{12}(\alpha,\beta) = 2\pi S_x(\beta)H_1(\beta)H_2^*(\beta)\delta(\beta - \alpha), \tag{3}$$

where

$$H(\omega;t) = \frac{e^{-i\omega t}}{2\pi}\int \Gamma(\omega,u)e^{iut}du \tag{4}$$

and $\delta(\alpha)$ is the Dirac delta function. Since the processes $\{y_1(t)\}$ and $\{y_2(t)\}$ are jointly wide sense stationary, there is no correlation between different frequencies. This is also demonstrated in equation (3) where the support of the 2-D spectrum $S_{12}(\alpha,\beta)$ is only on the $\alpha = \beta$ portion of the spectral coherence plane.

2.2 2-D SPECTRUM OF A SOURCE MOVING THROUGH AN OCEANIC WAVEGUIDE

In order to derive a useful bifrequency system function of an acoustic source moving through an oceanic waveguide with respect to a sensor, Hawker makes the linear motion model approximation. The schematic of this system is shown in figure 1, where $R(t)$ and $\theta(t)$ are time-dependent range and angles. In this approximation, the source is moving sufficiently slowly so that $R(t)$ and $\sin(\theta(t))$ can be adequately represented by the linear terms of the expansions about some region of time, Δ_t, centered at $t = t_o$ as

$$\begin{gathered} R(t) \approx R(t_o) + (t-t_o)R'(t_o) \\ \text{and} \\ \sin(\theta(t)) \approx \sin(\theta(t_o)) + (t-t_o)\theta'(t_o)\cos(\theta(t_o). \end{gathered} \tag{5}$$

Using the assumption that the acoustic propagation environment is cylindrically symmetric, Hawker shows that the bifrequency system function is given by

$$\Gamma(\omega,u) = \frac{\Delta_t}{\sqrt{8\pi}}e^{-i(u-\omega)t_o}e^{-i\pi/4}\sum_n \frac{Z_n(z_s)Z_n(z)}{\sqrt{k_nR_o}}\exp\left[-ik_nR_o\left(1-\frac{\nu}{\nu_n{}^g}\sin(\theta_o)\right)\right]\operatorname{sinc}(\nu_n\Delta_t/2)e^{-\alpha_nR_o}e^{-i(A_n-\omega)M_D} \tag{6}$$

where

Z_n = n^{th} modal depth eigenfunction
k_n = n^{th} modal eigenvalue
$\nu_n{}^g$ = n^{th} modal group velocity
α_n = n^{th} modal attenuation term
ν = source speed
z_s = source depth
M_D = delay associated with first modal arrival time,

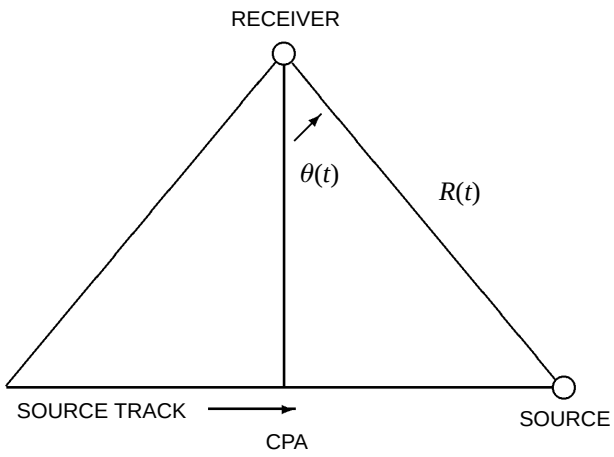

Figure 1. Source/receiver track scenario.

with $R_o = R(t_o)$, $\theta_o = \theta(t_o)$, $A_n = k_n \nu \sin(\theta_o) - k_n \nu^2 / \nu_n{}^g$, and $\nu_n = u - \omega + A_n$. For notational simplicity, the explicit dependence of these variables on ω is suppressed.

First, without loss of generality, we set $t_o = 0$. For analysis purposes, we let $\Delta_t \to \infty$ in equation (6). Then, using the identity

$$\lim_{\Delta_t \to \infty} \Delta_t \operatorname{sinc}(\nu_n \Delta_t / 2) = 2\pi\delta(\nu_n) , \tag{7}$$

we get

$$\Gamma(\omega, u) = \sqrt{\frac{\pi}{2}} e^{-i\pi/4} \sum_n \frac{Z_n(z_s) Z_n(z)}{\sqrt{k_n R_o}} \exp\left[-ik_n R_o \left(1 - \frac{\nu}{\nu_n}{}^g \sin(\theta_o) \right) \right] \sigma(\nu_n) e^{-\alpha_n R_o} e^{-i(A_n - \omega) M_D} . \tag{8}$$

Now, using equation (8) in equation (2) and grouping components dependent on ω into a modal dependent term $E_{n,m(\omega)}$, we get

$$S_{12}(\alpha, \beta) = \sum_n \sum_m \int E_{n,m}(\omega) \delta(\alpha - \omega + A_{1n}) \delta(\beta - \omega + A_{2m}) d\omega , \tag{9}$$

where the modal sums in equation (9) are assumed to be finite. Next, let

$$I_{n,m}(\alpha, \beta) = \int E_{n,m}(\omega) \delta(\alpha - \omega + A_{1n}) \delta(\beta - \omega + A_{2m}) d\omega . \tag{10}$$

Proceeding as in Papoulis (1962), we interpret $I_{n,m}(\alpha, \beta)$ as a distribution. Then we evaluate the integral

$$\int I_{n,m}(\alpha, \beta) \phi(\beta) d\beta = \int \int E_{n,m}(\omega) \delta(\alpha - \omega + A_{1n}) \delta(\beta - \omega + A_{2m}) \phi(\beta) d\omega d\beta , \tag{11}$$

where $\phi(\beta)$ is a continuous test function. After exchanging the order of integration, we get

$$\int I_{n,m}(\alpha,\beta)\phi(\beta)d\beta = \int E_{n,m}(\omega)\delta(\alpha - \omega + A_{1n})\phi(\omega - A_{2m})d\omega. \tag{12}$$

Next, we approximate A_{1n} and A_{2m} with the linear terms of the Taylor series expansion around a frequency ω_c within the band of interest as

$$A_{1n} \approx A_{1n}(\omega_c) + A'_{1n}(\omega_c)(\omega - \omega_c). \tag{13}$$

Then, using the fact that $A_{1n}(\omega_c) - A'_{1n}(\omega_c)\omega_c = 0$ and after a little manipulation we get

$$\int I_{n,m}(\alpha,\beta)\phi(\beta)d\beta = \frac{1}{\| 1 - A'_{1n} \|} E_{n,m}\left(\frac{\alpha}{1 - A'_{1n}}\right)\phi\left(\frac{1 - A'_{2m}}{1 - A'_{1n}}\alpha\right). \tag{14}$$

So, from equation (14) we conclude that

$$I_{n,m}(\alpha,\beta) = \frac{1}{\| 1 - A'_{1n} \|} E_{n,m}\left(\frac{\alpha}{1 - A'_{1n}}\right)\delta\left(\beta - \left(\frac{1 - A'_{2m}}{1 - A'_{1n}}\right)\alpha\right), \tag{15}$$

where

$$A'_{in} = \frac{v}{v_n}_g \sin(\theta_{oi}) + \left(\frac{v}{v_n}_g\right)^2 (k_n {v_n}'_g - 1). \tag{16}$$

And so the 2-D spectrum is given by

$$S_{12}(\alpha,\beta) = \sum_n \sum_m I_{n,m}(\alpha,\beta). \tag{17}$$

We see from equations (15) and (17) that $S_{12}(\alpha,\beta)$ only has support on regions of the (α,β)-spectral plane where $\beta = (1 - A'_{2m})/(1 - A'_{1n})\alpha$. From equation (16) we see that the slopes of these spectral lines are dependent on the source velocity with respect to each sensor as well as the acoustic propagation environment. The cross-modal spectral correlation is also evident.

2.3 2-D SPECTRAL COHERENCE

The structure of the 2-D spectrum in equations (15) and (17) lends itself to an estimation procedure first introduced by Hurd & Gerr (1991) for the spectral analysis of cyclostationary processes and adapted by Allen to include the Doppler processing of moving targets in a plane-wave propagation environment (Allen & Hobbs, 1992, 1993).

The procedure involves forming the outer product of the short-time Fourier transform of the sampled data from each sensor and smoothing along lines corresponding to potential source-sensor

trajectories. This method forms a consistent estimate $\hat{S}_{12}(\alpha,\beta)$ of the sum of the coefficients of the delta functions in equation (15). The 2-D spectral coherence then is defined as (Gerr & Allen, 1994).

$$C_{12}(\alpha,\beta) = \frac{\hat{S}_{12}(\alpha,\beta)}{\left[\hat{S}_{11}(\alpha,\alpha)\hat{S}_{22}(\beta,\beta)\right]^{1/2}}. \tag{18}$$

3. EXPERIMENTAL RESULTS

In this section we demonstrate the spectral analysis technique from section 2.3 on a real data set. We analyzed a portion of data collected during the SWellEX-3 experiment that was held during July and August of 1994 in the Southern California Shallow-Water Testbed (SWTB). This experiment was meant to test the passive detection of targets in a shallow-water environment (50 to 200 m).

3.1 DATA SET DESCRIPTION

The SWellEX-3 data that were analyzed were part of the Short-Range CPA Event. We used 30 minutes of data collected from hydrophone 2 of node 2 (sensor 1) and hydrophone 131 of node 5 (sensor 2) of the Shallow-Water Sensor String (SWSS) horizontal line array. Both hydrophones are of type HF(5–1040 Hz}). The bottom-mounted array was deployed at a depth of approximately 170 to 180 m. The environmental information is displayed in appendix A (Baxley & Booth, 1995) in the form of a KRAKEN (Porter, 1991) environmental input file for an adjacent region. Figure 2 is a schematic of the data set, which includes the relative sensor locations and the source track determined from Global Positioning System (GPS) data. The broadband source was produced by a pseudo-random noise generator and was towed at a speed of approximately 1.54 m/s at a nominal depth of 60 m. The spectrograms of the two hydrophones are given in figures 3 and 4 over the 400- to 800-Hz frequency range.

3.2 SPECTRAL ANALYSIS RESULTS

We present results from three principle subsections of this data set labeled A, B, and C in figure 2. They represent varying degrees of relative range-rate with respect to the sensors. Section A is at the beginning of the data set and corresponds to the least amount of relative Doppler offset between the two sensors. Section C represents the most severe case. Appendix B contains the MATLAB code used to calculate the 2-D spectral coherence.

In the spectral analysis results presented in this section, it was necessary to eliminate an estimate of the “coarse time delay” associated with the difference in propagation time between the two sensors. This is because this estimation procedure is based upon a spectral smoothing approach and so is very sensitive to the phase introduced by the propagation delay (Gerr & Allen, 1994).

Figures 5, 7, and 9 are the 2-D spectral coherence for the three data sections over the 660- to 670-Hz band generated from 15.7 seconds of time series. The α-coordinate is on the vertical axis. To more clearly display the frequency offset of the spectral correlation structure, figures 11 and 13 display the 2-D spectral coherence of data sections B and C over the 660- to 665-Hz frequency band. Figures 6, 8, 10, 12, and 14 are the corresponding analytical regions of support generated with the results of section 2 using 22 modes and using KRAKEN with the environmental information given in appendix A. Only the potential regions of support are plotted using equation (15) and not the actual

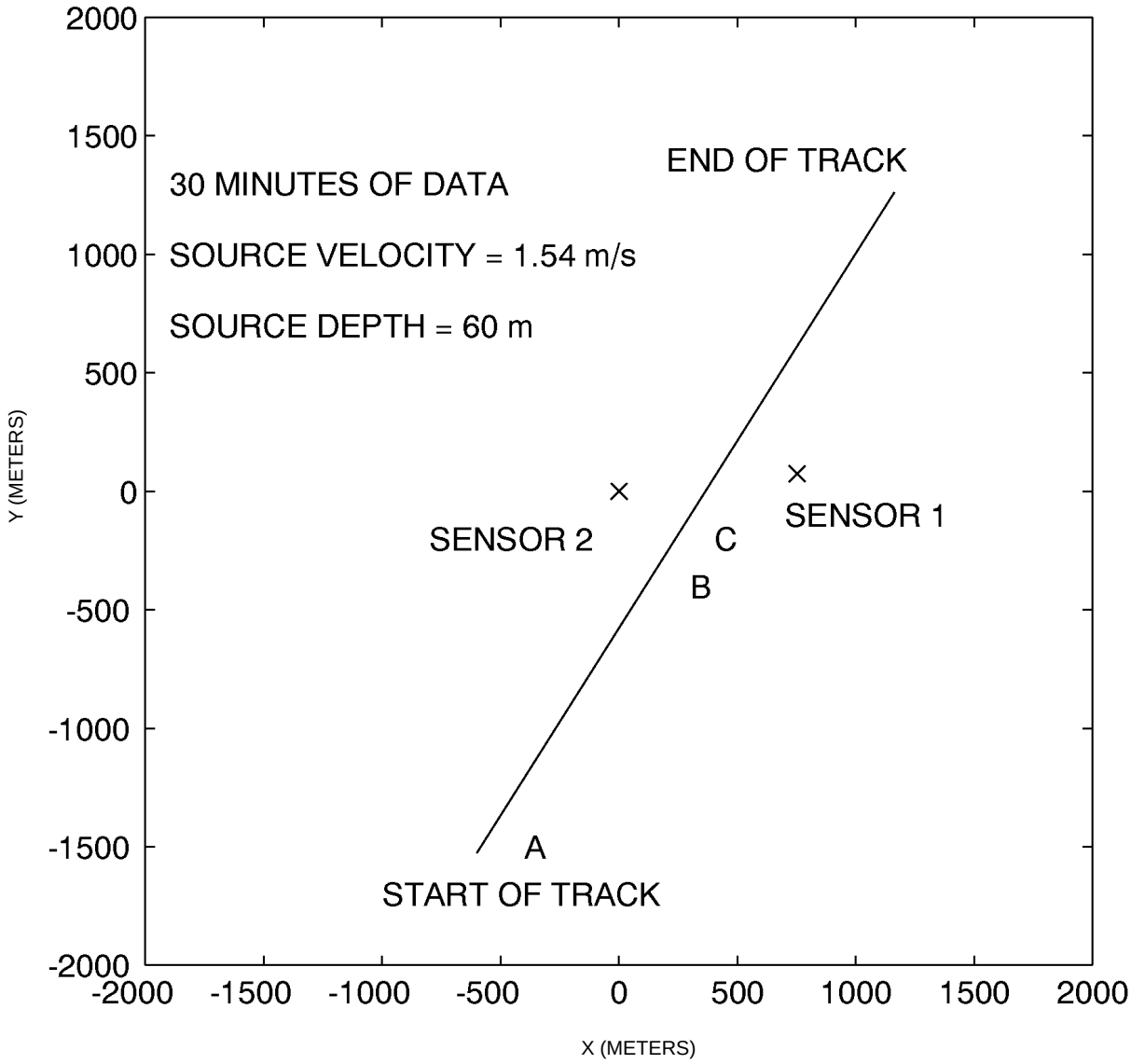

Figure 2. Source track and sensor geometry.

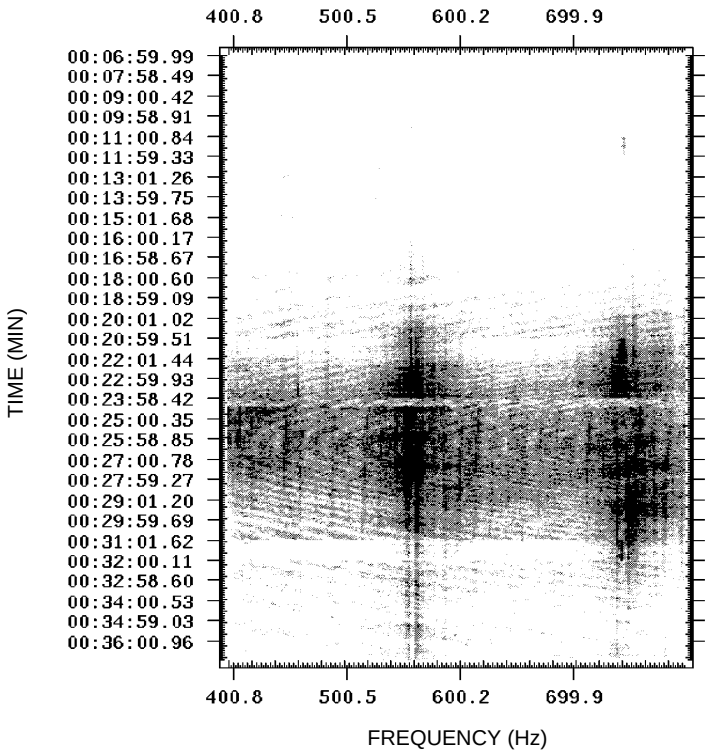

Figure 3. Spectrogram of channel 1.

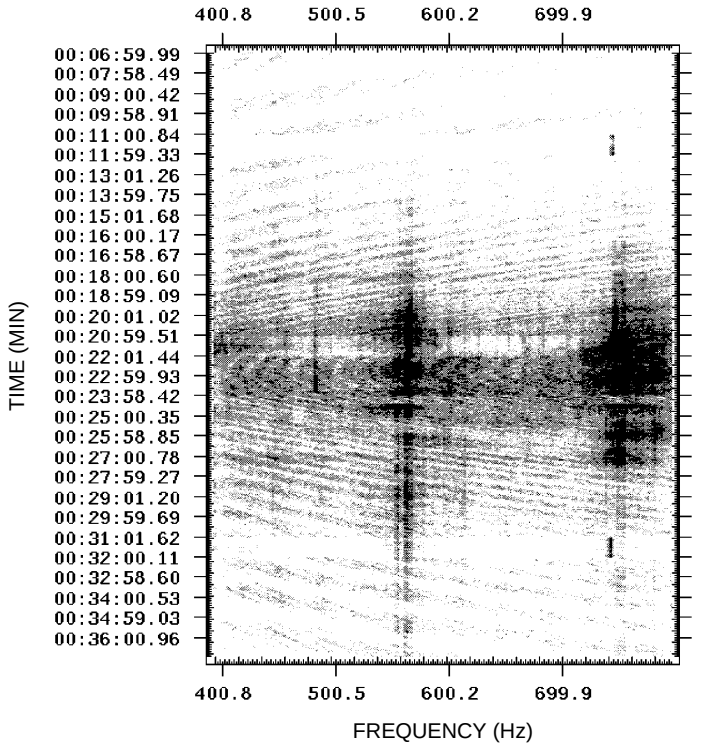

Figure 4. Spectrogram of channel 2.

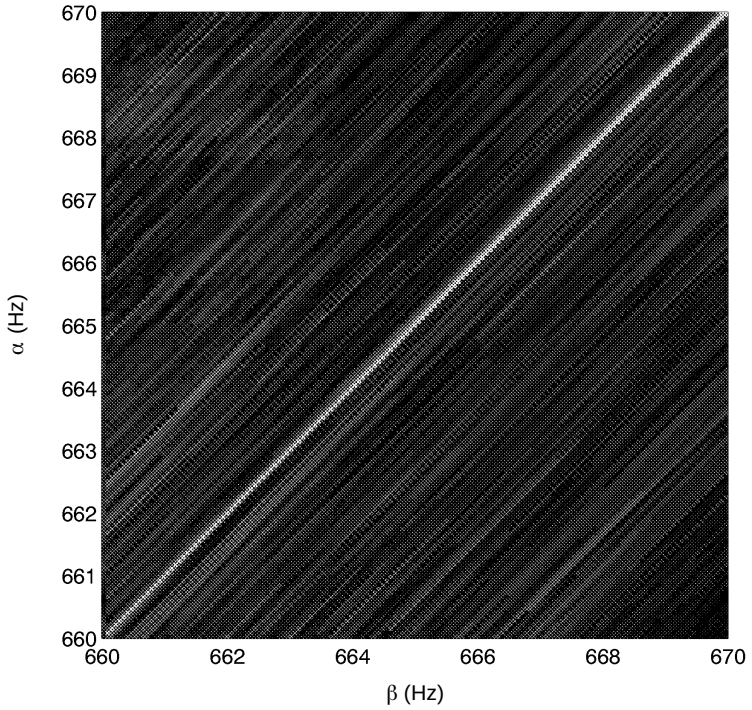

Figure 5. 2-D spectral coherence for section A over 660- to 670-Hz band.

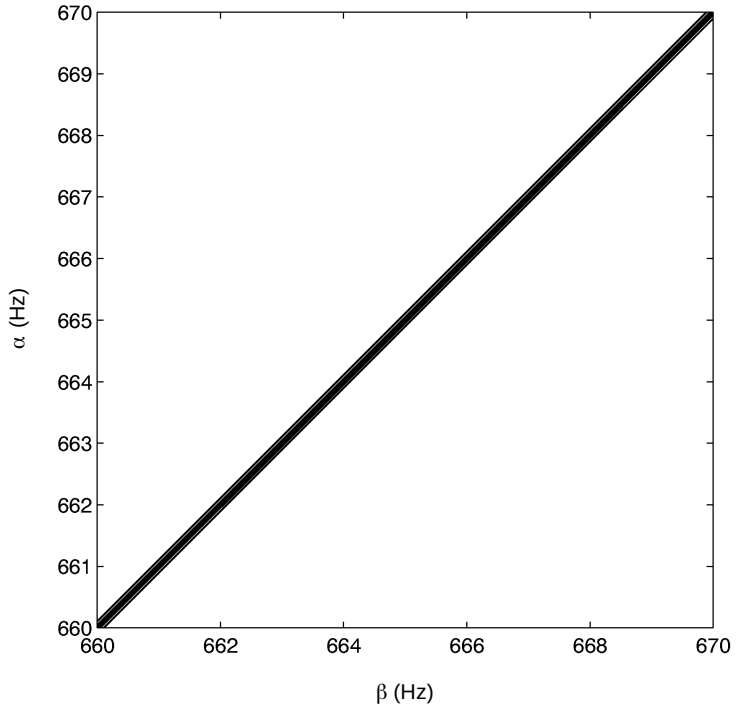

Figure 6. Analytical region of support of 2-D spectral coherence for section A over 660- to 670-Hz band.

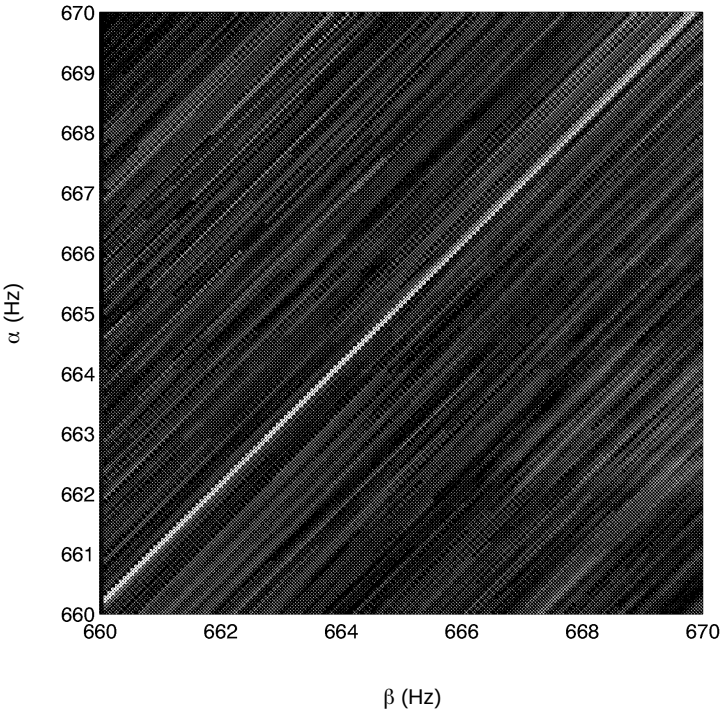

Figure 7. 2-D spectral coherence for section B over 660- to 670-Hz band.

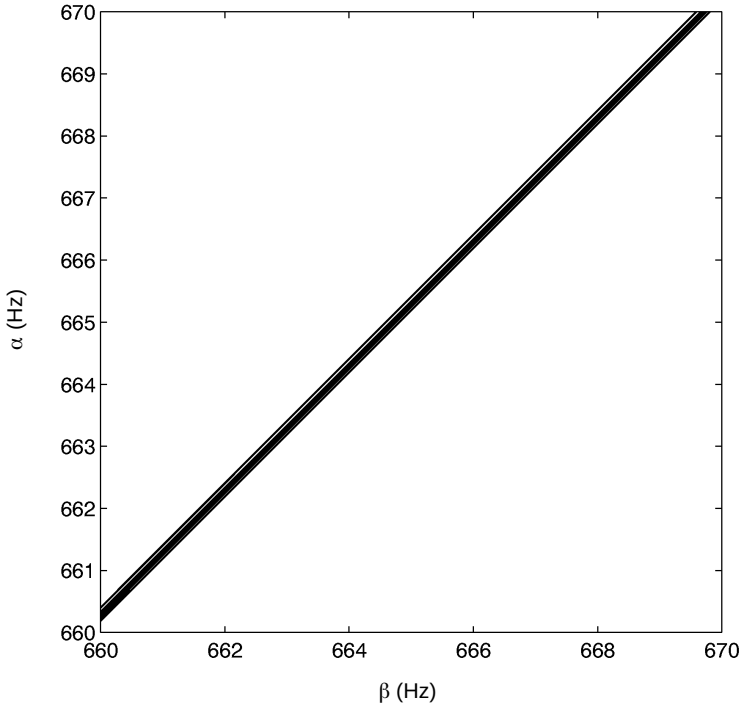

Figure 8. Analytical region of support of 2-D spectral coherence for section B over 660- to 670-Hz band.

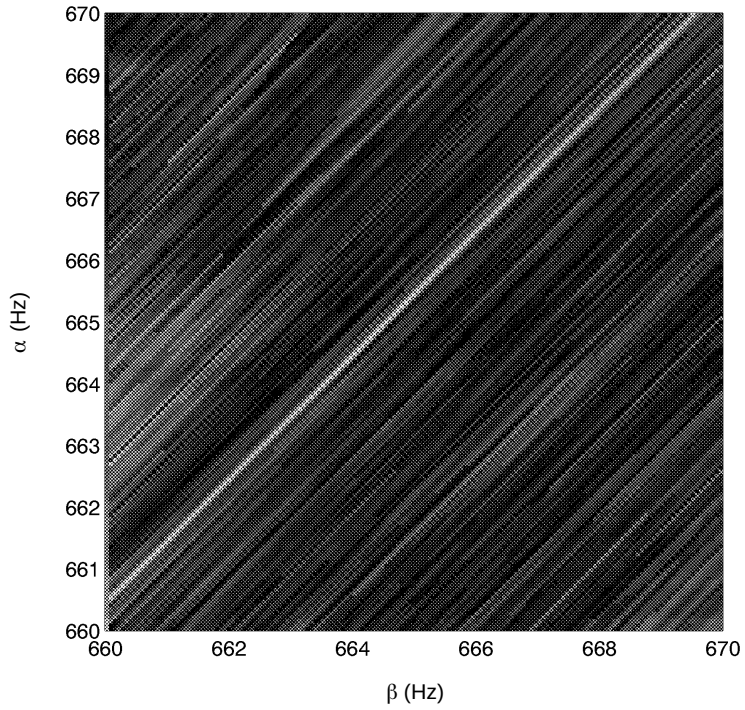

Figure 9. 2-D spectral coherence for section C over 660- to 670-Hz band.

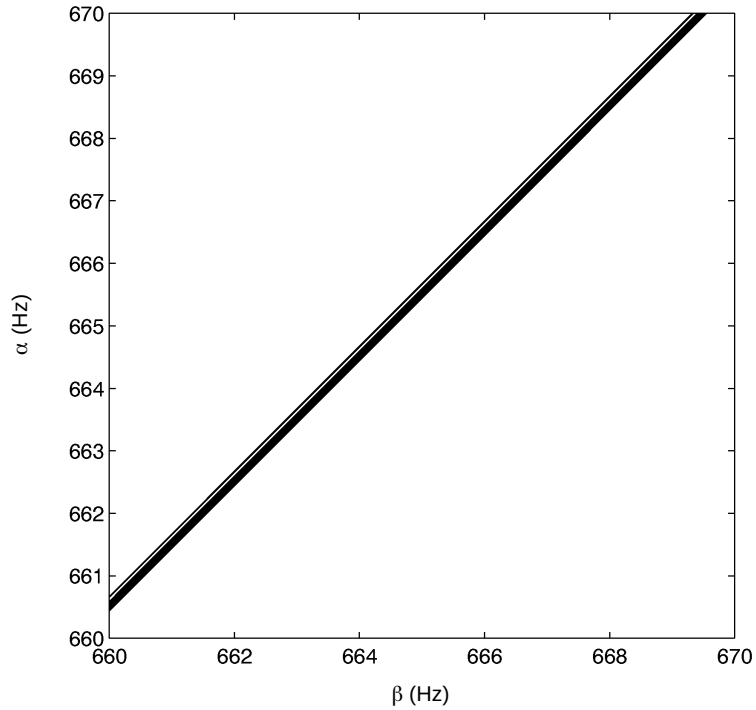

Figure 10. Analytical region of support of 2-D spectral coherence for section C over 660- to 670-Hz band.

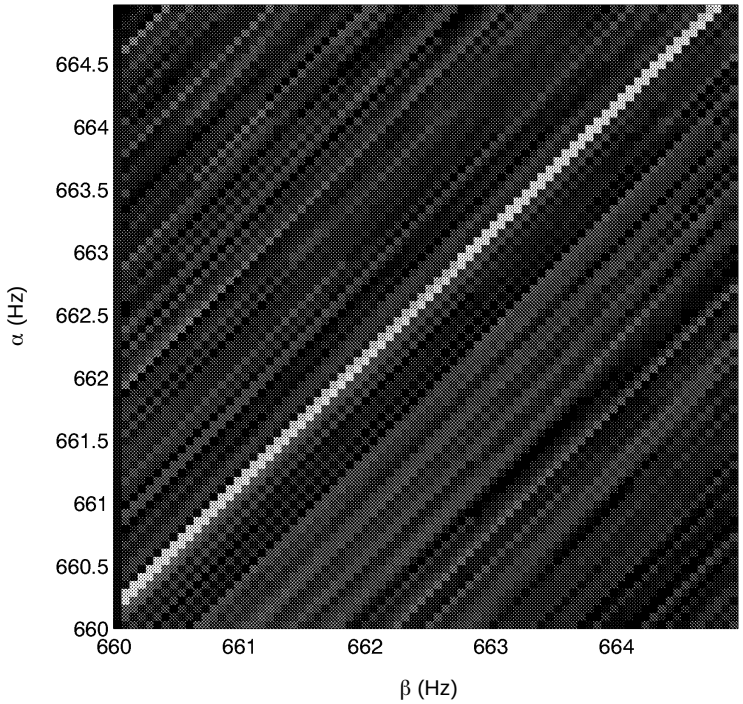

Figure 11. 2-D spectral coherence for section B over 660- to 665-Hz band.

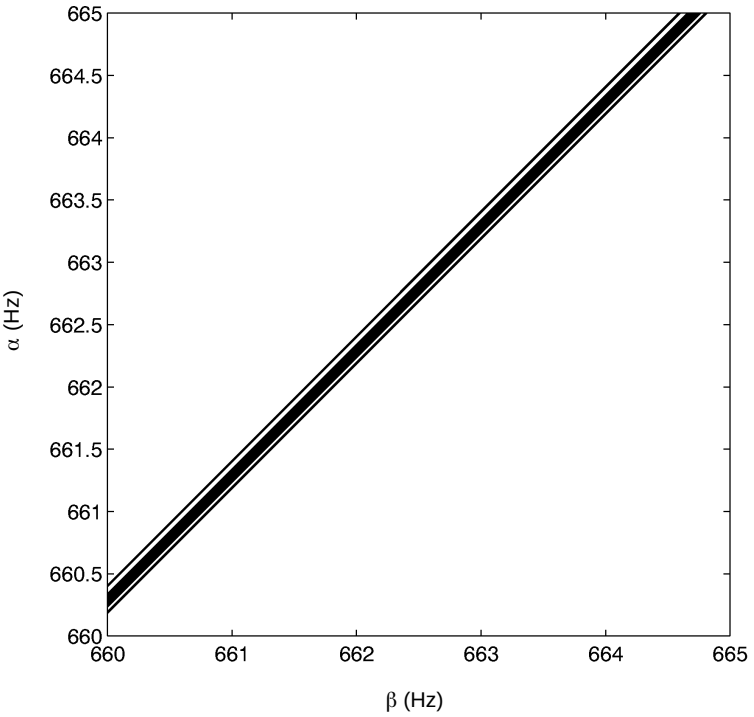

Figure 12. Analytical region of support of 2-D spectral coherence for section B over 660- to 665-Hz band.

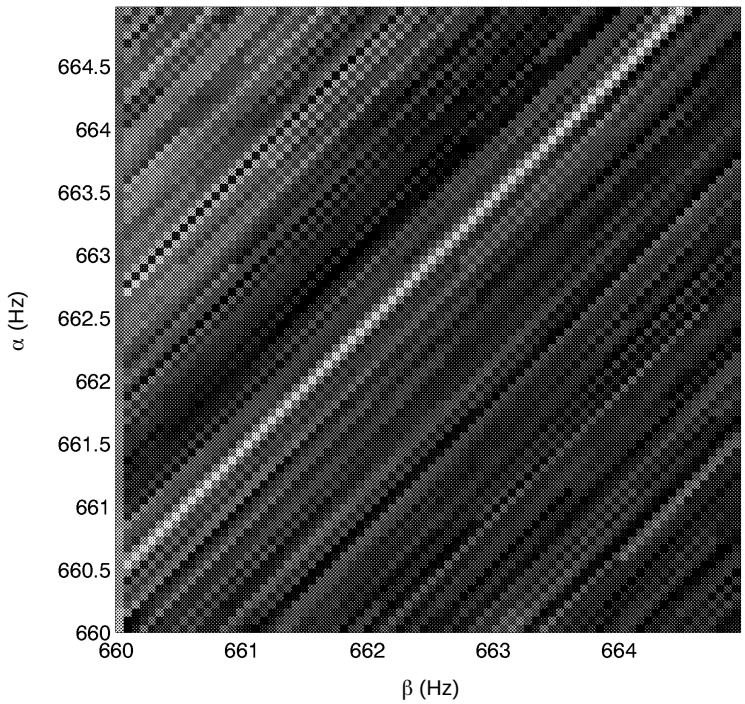

Figure 13. 2-D spectral coherence for section C over 660- to 665-Hz band.

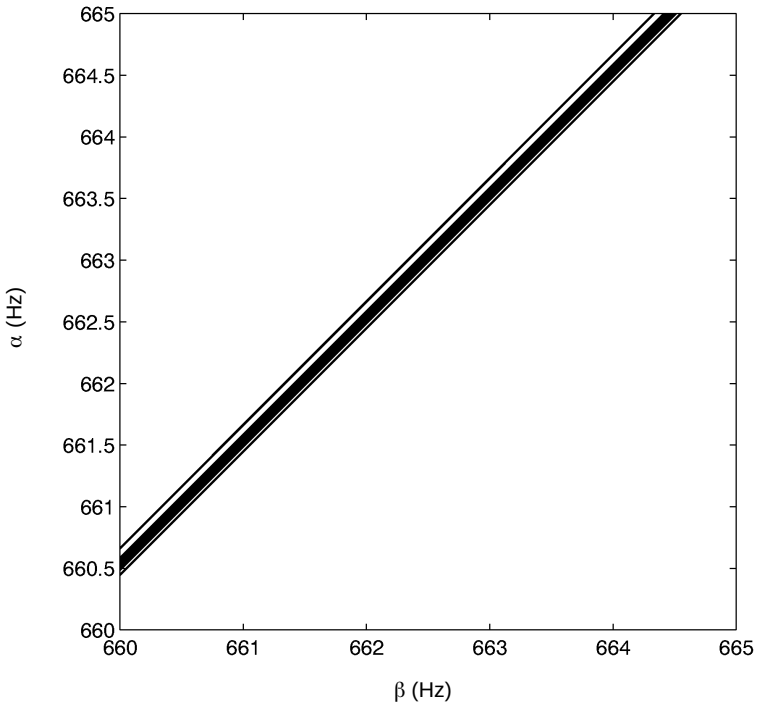

Figure 14. Analytical region of support of 2-D spectral coherence for section C over 660- to 665-Hz band.

2-D spectral coherence. Since no summing is being done, many more potential cross-modal lines are plotted in these figures. However, they are in approximate agreement with the corresponding estimated plots. Discrepancies are probably due to the inaccuracy of the environmental information and the fact that the actual propagation environment for this site is not range-independent as assumed in the analysis of section 2. The spectral correlation due to source motion is clearly evident in the plots.

One of the primary attributes of spectral coherence processing is that it allows for very long Fourier transforms to be taken. This is in contrast to conventional spectral estimation that requires the source to be approximately stationary over the data length of the transform. Since source motion is inherently accounted for in the spectral coherence estimation procedure, this type of processing accommodates much longer transform lengths. Figure 15 is the estimated 2-D spectral coherence over the 660- to 660.625-Hz frequency band for data section A generated from 251.7 seconds of time series. Figure 16 is the corresponding analytical region of support. Much finer spectral coherence detail is evident in these plots as opposed to the detail afforded by the 15.7-second transform represented in figures 5 and 6 over the wider frequency range. We see interesting auto- and cross-modal spectral correlation from these plots. However, this length of Fourier transform would be inappropriate for the shorter-range sections, B and C, since the linear motion model would be invalid in these sections over this length of time.

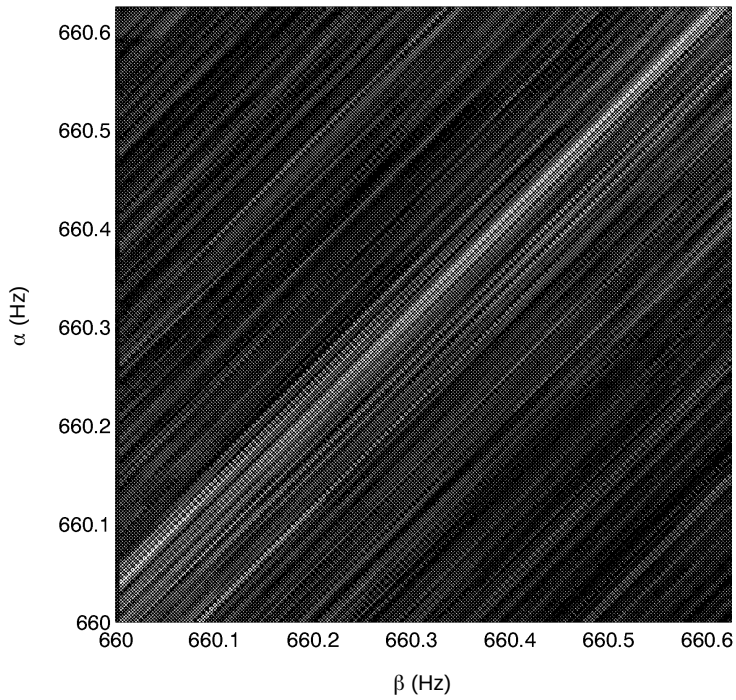

Figure 15. 2-D spectral coherence for section A over 660- to 660.625-Hz band.

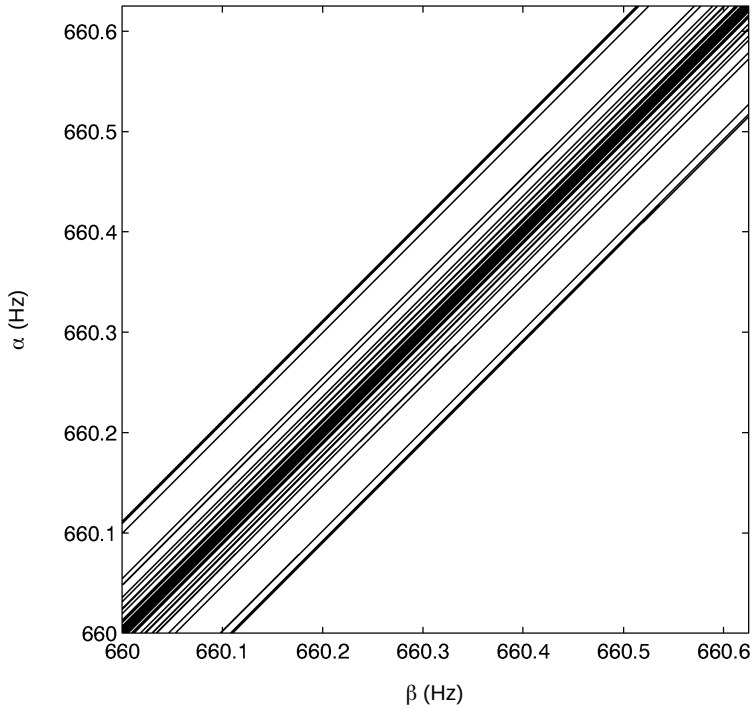

Figure 16. Analytical region of support of 2-D spectral coherence for section A over 660- to 660.625-Hz band.

4. CONCLUSION

In this document we derived the 2-D spectrum of a broadband source moving through an oceanic waveguide. The 2-D spectrum describes the spectral correlation structure of the time series received at two sensors due to a moving source. We demonstrated how its structure is dependent on the source velocity with respect to the sensors as well as the acoustic propagation environment.

We also showed that this structure lends itself to an established spectral smoothing procedure that was shown to be a consistent estimator of the 2-D spectral coherence. We then applied this technique to a real data set collected during the SWellEX-3 experiment and demonstrated how the theoretical spectral coherence approximates the experimental.

5. RECOMMENDATIONS

The most critical issue in using the results presented in this document is the estimation procedure. Further work should be done to test the robustness of the spectral smoothing technique. For instance, it should be tested in an environment in which there is a strong interference overlapping the band of the desired source. The effect of near- and far-field interferers on the estimation technique should be determined.

Several improvements can be made to the procedure applied to the underwater acoustic problem. An automated procedure should be developed that would accommodate many source ranges and velocities and simultaneously account for coarse time delay correction. Also, some effort should be expended to develop a computationally efficient implementation.

Finally, a method can be developed to incorporate 2-D spectral coherence into an array-processing algorithm to enhance the detection and localization of moving targets. This should be completely analogous to power spectral density use in frequency-domain, array-processing algorithms. The theoretical 2-D spectrum should also be derived for a range-dependent propagation environment.

6. REFERENCES

Allen, J. C. and S. L. Hobbs. 1992. “Detecting Target Motion by Frequency-Plane Smoothing,” *26th Asilomar Conference on Signals, Systems & Computers* (pp. 1042–1047). 26–28 Oct 1992, Pacific Grove, CA. IEEE Computer Society Press.

Allen, J. C. and S. L. Hobbs. 1993. “Instantaneous Variance Estimation by Spectral Collapse,” *27th Asilomar Conference on Signals, Systems & Computers* (pp. 1128–1132). 1–3 Nov, Pacific Grove, CA. IEEE Computer Society Press.

Baxley, P. A. and N. O. Booth. 1995. “Matched-Field Replica Model Optimization and Bottom Property Inversion Using Multitone Signals in Shallow Water,” *Journal of the Acoustical Society of America*, vol. 97 (May), no. 5, pp. 3290–3291.

Gerr, N. L. and J. C. Allen. 1994. “Time-Delay Estimation for Harmonizable Signals,” *Digital Signal Processing*,” vol. 4 (Jan), no. 1, pp. 49–62.

Hawker, K. E. 1979. “A Normal Mode Theory of Acoustic Doppler Effects in the Oceanic Waveguide,” *Journal of the Acoustical Society of America*, vol. 65, no. 3, pp. 675–681 (Mar).

Hurd, H. L. 1989. “Representation of Strongly Harmonizable Periodically Correlated Processes and Their Covariances,” *Journal of Multivariate Analysis*, vol. 29 (Apr), no. 1, pp. 53–67.

Hurd, H. L. and N. L. Gerr. 1991. “Time-Delay Estimation for Harmonizable Signals,” *Journal of Time Series Analysis*, vol. 12, no. 4, pp. 337–350.

Papoulis, A. 1962. *The Fourier Integral and Its Applications*, pp. 269–282. McGraw–Hill, New York, New York.

Porter, M. B. 1991. “The KRAKEN Normal Mode Program,” Supreme Allied Command Atlantic (SACLANT) Undersea Research Centre, SM–245 edition. La Spezia, Italy.

Reuter, M. 1994. “Characterization and Simulation of an Acoustic Source Moving Through an Oceanic Waveguide,” NRaD TR 1673. Naval Command, Control and Ocean Surveillance Center RDT&E Division, San Diego, CA.

Zadeh, L. A. 1950. “Frequency Analysis of Variable Networks,” *Proceedings of the Institute of Radio Engineers*, vol. 38, pp. 291–299 (Mar).

APPENDIX A
EXPERIMENT SITE ENVIRONMENTAL INFORMATION

This appendix contains the nominal KRAKEN environmental file for the SWellEX-3 experiment.

```
"SWELLEX-3"
10
3
'NVF.'
400  0.0  198.0
   0.0  1522.610  0.0  1.0  4.55578E-06  0.0        47.0  1497.400  0.0  1.0  4.55578E-06  0.0
   1.0  1523.110  0.0  1.0  4.55578E-06  0.0        48.0  1497.150  0.0  1.0  4.55578E-06  0.0
   2.0  1523.180  0.0  1.0  4.55578E-06  0.0        49.0  1497.050  0.0  1.0  4.55578E-06  0.0
   3.0  1523.230  0.0  1.0  4.55578E-06  0.0        50.0  1496.860  0.0  1.0  4.55578E-06  0.0
   4.0  1523.020  0.0  1.0  4.55578E-06  0.0        51.0  1496.360  0.0  1.0  4.55578E-06  0.0
   5.0  1522.770  0.0  1.0  4.55578E-06  0.0        52.0  1496.280  0.0  1.0  4.55578E-06  0.0
   6.0  1522.230  0.0  1.0  4.55578E-06  0.0        53.0  1496.170  0.0  1.0  4.55578E-06  0.0
   7.0  1521.110  0.0  1.0  4.55578E-06  0.0        54.0  1495.960  0.0  1.0  4.55578E-06  0.0
   8.0  1520.380  0.0  1.0  4.55578E-06  0.0        55.0  1495.600  0.0  1.0  4.55578E-06  0.0
   9.0  1519.650  0.0  1.0  4.55578E-06  0.0        56.0  1495.610  0.0  1.0  4.55578E-06  0.0
  10.0  1518.720  0.0  1.0  4.55578E-06  0.0        57.0  1495.550  0.0  1.0  4.55578E-06  0.0
  11.0  1518.190  0.0  1.0  4.55578E-06  0.0        58.0  1495.330  0.0  1.0  4.55578E-06  0.0
  12.0  1518.170  0.0  1.0  4.55578E-06  0.0        59.0  1494.940  0.0  1.0  4.55578E-06  0.0
  13.0  1515.900  0.0  1.0  4.55578E-06  0.0        60.0  1494.690  0.0  1.0  4.55578E-06  0.0
  14.0  1515.460  0.0  1.0  4.55578E-06  0.0        61.0  1494.550  0.0  1.0  4.55578E-06  0.0
  15.0  1514.190  0.0  1.0  4.55578E-06  0.0        62.0  1494.330  0.0  1.0  4.55578E-06  0.0
  16.0  1514.040  0.0  1.0  4.55578E-06  0.0        63.0  1494.080  0.0  1.0  4.55578E-06  0.0
  17.0  1513.300  0.0  1.0  4.55578E-06  0.0        64.0  1493.950  0.0  1.0  4.55578E-06  0.0
  18.0  1511.930  0.0  1.0  4.55578E-06  0.0        65.0  1494.160  0.0  1.0  4.55578E-06  0.0
  19.0  1510.970  0.0  1.0  4.55578E-06  0.0        66.0  1493.880  0.0  1.0  4.55578E-06  0.0
  20.0  1509.710  0.0  1.0  4.55578E-06  0.0        67.0  1494.100  0.0  1.0  4.55578E-06  0.0
  21.0  1509.290  0.0  1.0  4.55578E-06  0.0        68.0  1493.970  0.0  1.0  4.55578E-06  0.0
  22.0  1508.800  0.0  1.0  4.55578E-06  0.0        69.0  1493.880  0.0  1.0  4.55578E-06  0.0
  23.0  1508.110  0.0  1.0  4.55578E-06  0.0        70.0  1493.940  0.0  1.0  4.55578E-06  0.0
  24.0  1504.960  0.0  1.0  4.55578E-06  0.0        71.0  1493.580  0.0  1.0  4.55578E-06  0.0
  25.0  1505.510  0.0  1.0  4.55578E-06  0.0        72.0  1493.420  0.0  1.0  4.55578E-06  0.0
  26.0  1503.730  0.0  1.0  4.55578E-06  0.0        73.0  1494.060  0.0  1.0  4.55578E-06  0.0
  27.0  1502.710  0.0  1.0  4.55578E-06  0.0        74.0  1493.600  0.0  1.0  4.55578E-06  0.0
  28.0  1502.310  0.0  1.0  4.55578E-06  0.0        75.0  1493.550  0.0  1.0  4.55578E-06  0.0
  29.0  1501.100  0.0  1.0  4.55578E-06  0.0        76.0  1493.050  0.0  1.0  4.55578E-06  0.0
  30.0  1500.210  0.0  1.0  4.55578E-06  0.0        77.0  1493.010  0.0  1.0  4.55578E-06  0.0
  31.0  1500.120  0.0  1.0  4.55578E-06  0.0        78.0  1492.780  0.0  1.0  4.55578E-06  0.0
  32.0  1500.200  0.0  1.0  4.55578E-06  0.0        79.0  1492.560  0.0  1.0  4.55578E-06  0.0
  33.0  1500.000  0.0  1.0  4.55578E-06  0.0        80.0  1492.280  0.0  1.0  4.55578E-06  0.0
  34.0  1499.580  0.0  1.0  4.55578E-06  0.0        81.0  1492.210  0.0  1.0  4.55578E-06  0.0
  35.0  1499.160  0.0  1.0  4.55578E-06  0.0        82.0  1492.210  0.0  1.0  4.55578E-06  0.0
  36.0  1498.740  0.0  1.0  4.55578E-06  0.0        83.0  1492.120  0.0  1.0  4.55578E-06  0.0
  37.0  1498.810  0.0  1.0  4.55578E-06  0.0        84.0  1491.910  0.0  1.0  4.55578E-06  0.0
  38.0  1498.570  0.0  1.0  4.55578E-06  0.0        85.0  1491.890  0.0  1.0  4.55578E-06  0.0
  39.0  1498.110  0.0  1.0  4.55578E-06  0.0        86.0  1491.860  0.0  1.0  4.55578E-06  0.0
  40.0  1498.030  0.0  1.0  4.55578E-06  0.0        87.0  1491.850  0.0  1.0  4.55578E-06  0.0
  41.0  1497.940  0.0  1.0  4.55578E-06  0.0        88.0  1491.760  0.0  1.0  4.55578E-06  0.0
  42.0  1498.130  0.0  1.0  4.55578E-06  0.0        89.0  1491.680  0.0  1.0  4.55578E-06  0.0
  43.0  1498.030  0.0  1.0  4.55578E-06  0.0        90.0  1491.650  0.0  1.0  4.55578E-06  0.0
  44.0  1497.590  0.0  1.0  4.55578E-06  0.0        91.0  1491.640  0.0  1.0  4.55578E-06  0.0
  45.0  1497.670  0.0  1.0  4.55578E-06  0.0        92.0  1491.630  0.0  1.0  4.55578E-06  0.0
  46.0  1497.210  0.0  1.0  4.55578E-06  0.0        93.0  1491.440  0.0  1.0  4.55578E-06  0.0
```

94.0	1491.470	0.0	1.0	4.55578E-06	0.0	149.0	1490.990	0.0	1.0	4.55578E-06	0.0
95.0	1491.280	0.0	1.0	4.55578E-06	0.0	150.0	1490.970	0.0	1.0	4.55578E-06	0.0
96.0	1491.000	0.0	1.0	4.55578E-06	0.0	151.0	1490.960	0.0	1.0	4.55578E-06	0.0
97.0	1490.870	0.0	1.0	4.55578E-06	0.0	152.0	1490.960	0.0	1.0	4.55578E-06	0.0
98.0	1490.930	0.0	1.0	4.55578E-06	0.0	153.0	1490.970	0.0	1.0	4.55578E-06	0.0
99.0	1491.060	0.0	1.0	4.55578E-06	0.0	154.0	1490.980	0.0	1.0	4.55578E-06	0.0
100.0	1491.260	0.0	1.0	4.55578E-06	0.0	155.0	1490.940	0.0	1.0	4.55578E-06	0.0
101.0	1491.180	0.0	1.0	4.55578E-06	0.0	156.0	1490.970	0.0	1.0	4.55578E-06	0.0
102.0	1491.230	0.0	1.0	4.55578E-06	0.0	157.0	1490.980	0.0	1.0	4.55578E-06	0.0
103.0	1491.410	0.0	1.0	4.55578E-06	0.0	158.0	1490.960	0.0	1.0	4.55578E-06	0.0
104.0	1491.340	0.0	1.0	4.55578E-06	0.0	159.0	1490.940	0.0	1.0	4.55578E-06	0.0
105.0	1491.450	0.0	1.0	4.55578E-06	0.0	160.0	1490.980	0.0	1.0	4.55578E-06	0.0
106.0	1491.430	0.0	1.0	4.55578E-06	0.0	161.0	1490.980	0.0	1.0	4.55578E-06	0.0
107.0	1491.380	0.0	1.0	4.55578E-06	0.0	162.0	1490.950	0.0	1.0	4.55578E-06	0.0
108.0	1491.350	0.0	1.0	4.55578E-06	0.0	163.0	1490.960	0.0	1.0	4.55578E-06	0.0
109.0	1491.340	0.0	1.0	4.55578E-06	0.0	164.0	1490.940	0.0	1.0	4.55578E-06	0.0
110.0	1491.450	0.0	1.0	4.55578E-06	0.0	165.0	1490.940	0.0	1.0	4.55578E-06	0.0
111.0	1491.520	0.0	1.0	4.55578E-06	0.0	166.0	1490.950	0.0	1.0	4.55578E-06	0.0
112.0	1491.510	0.0	1.0	4.55578E-06	0.0	167.0	1490.950	0.0	1.0	4.55578E-06	0.0
113.0	1491.500	0.0	1.0	4.55578E-06	0.0	168.0	1490.870	0.0	1.0	4.55578E-06	0.0
114.0	1491.370	0.0	1.0	4.55578E-06	0.0	169.0	1490.860	0.0	1.0	4.55578E-06	0.0
115.0	1491.290	0.0	1.0	4.55578E-06	0.0	170.0	1490.860	0.0	1.0	4.55578E-06	0.0
116.0	1491.400	0.0	1.0	4.55578E-06	0.0	171.0	1490.840	0.0	1.0	4.55578E-06	0.0
117.0	1491.290	0.0	1.0	4.55578E-06	0.0	172.0	1490.810	0.0	1.0	4.55578E-06	0.0
118.0	1491.380	0.0	1.0	4.55578E-06	0.0	173.0	1490.780	0.0	1.0	4.55578E-06	0.0
119.0	1491.430	0.0	1.0	4.55578E-06	0.0	174.0	1490.760	0.0	1.0	4.55578E-06	0.0
120.0	1491.330	0.0	1.0	4.55578E-06	0.0	175.0	1490.720	0.0	1.0	4.55578E-06	0.0
121.0	1491.280	0.0	1.0	4.55578E-06	0.0	176.0	1490.710	0.0	1.0	4.55578E-06	0.0
122.0	1491.210	0.0	1.0	4.55578E-06	0.0	177.0	1490.740	0.0	1.0	4.55578E-06	0.0
123.0	1491.230	0.0	1.0	4.55578E-06	0.0	178.0	1490.720	0.0	1.0	4.55578E-06	0.0
124.0	1491.120	0.0	1.0	4.55578E-06	0.0	179.0	1490.760	0.0	1.0	4.55578E-06	0.0
125.0	1491.130	0.0	1.0	4.55578E-06	0.0	180.0	1490.780	0.0	1.0	4.55578E-06	0.0
126.0	1491.190	0.0	1.0	4.55578E-06	0.0	181.0	1490.800	0.0	1.0	4.55578E-06	0.0
127.0	1491.160	0.0	1.0	4.55578E-06	0.0	182.0	1490.810	0.0	1.0	4.55578E-06	0.0
128.0	1491.110	0.0	1.0	4.55578E-06	0.0	183.0	1490.810	0.0	1.0	4.55578E-06	0.0
129.0	1491.180	0.0	1.0	4.55578E-06	0.0	184.0	1490.740	0.0	1.0	4.55578E-06	0.0
130.0	1491.170	0.0	1.0	4.55578E-06	0.0	185.0	1490.730	0.0	1.0	4.55578E-06	0.0
131.0	1491.130	0.0	1.0	4.55578E-06	0.0	186.0	1490.690	0.0	1.0	4.55578E-06	0.0
132.0	1491.090	0.0	1.0	4.55578E-06	0.0	187.0	1490.640	0.0	1.0	4.55578E-06	0.0
133.0	1491.030	0.0	1.0	4.55578E-06	0.0	188.0	1490.610	0.0	1.0	4.55578E-06	0.0
134.0	1490.980	0.0	1.0	4.55578E-06	0.0	189.0	1490.580	0.0	1.0	4.55578E-06	0.0
135.0	1490.930	0.0	1.0	4.55578E-06	0.0	190.0	1490.560	0.0	1.0	4.55578E-06	0.0
136.0	1490.900	0.0	1.0	4.55578E-06	0.0	191.0	1490.860	0.0	1.0	4.55578E-06	0.0
137.0	1490.880	0.0	1.0	4.55578E-06	0.0	192.0	1490.940	0.0	1.0	4.55578E-06	0.0
138.0	1490.890	0.0	1.0	4.55578E-06	0.0	193.0	1490.990	0.0	1.0	4.55578E-06	0.0
139.0	1490.910	0.0	1.0	4.55578E-06	0.0	194.0	1491.010	0.0	1.0	4.55578E-06	0.0
140.0	1490.940	0.0	1.0	4.55578E-06	0.0	195.0	1491.030	0.0	1.0	4.55578E-06	0.0
141.0	1490.950	0.0	1.0	4.55578E-06	0.0	196.0	1491.040	0.0	1.0	4.55578E-06	0.0
142.0	1490.940	0.0	1.0	4.55578E-06	0.0	197.0	1491.050	0.0	1.0	4.55578E-06	0.0
143.0	1490.960	0.0	1.0	4.55578E-06	0.0	198.0	1491.070	0.0	1.0	4.55578E-06	0.0
144.0	1490.950	0.0	1.0	4.55578E-06	0.0	500 0.0 228.0					
145.0	1490.940	0.0	1.0	4.55578E-06	0.0	198.00 1572.368 0.0 1.76 0.200 0.0					
146.0	1490.950	0.0	1.0	4.55578E-06	0.0	228.00 1593.016 0.0 1.76 0.200 0.0					
147.0	1490.970	0.0	1.0	4.55578E-06	0.0	1500 0.0 1028.0					
148.0	1490.970	0.0	1.0	4.55578E-06	0.0	228.00 1881.00 0.0 2.06 0.060 0.					

```
1500  0.0  1028.0
 228.00  1881.00   0.0  2.06  0.060  0.0
1028.00  3245.80   0.0  2.06  0.060  0.0
'A', 0.
1028.00, 5200.00   0.0  2.66  0.020  0.0
1490.0  5000.00
15.0
100 2.0 200.0 /
48 101.375 189.5 /
```

APPENDIX B
SPECTRAL ANALYSIS CODE

The two MATLAB*.m files shown in this appendix comprise the 2-D spectral coherence estimation algorithm used to generate the results in section 3. The function **make_index** is first called to construct the **INDX** matrix used to map between rectangular and polar coordinates. Then **bispec** is called to generate the 2-D spectral coherence function.

```
function [Indx,spec_size] = make_index(low_freq,high_freq,sr,fft_size)
% Function make_index
%       [INDX,SPEC_SIZE] = MAKE_INDEX(LOW_FREQ,HIGH_FREQ,SR,FFT_SIZE)
%       Computes the mapping matrix INDX which is used in the estimation
%       of spectral coherence.  INDX maps points on a rectangular grid
%       to polar coordinates.
%
% Variables
%       LOW_FREQ: Lowest frequency in spectral coherence plane
%       HIGH_FREQ: Highest frequency in spectral coherence plane
%       SR: Sample rate
%       FFT_SIZE: Length of FFT
%
%       INDX: Mapping matrix
%       SPEC_SIZE: Used to determine number of unique slopes
% Author: M. Reuter 9-5-95

% Set parameters and do sanity check
if low_freq >= high_freq
   disp(' ERROR: Requested low frequency is greater than the high frequency')
   return
end

all_size = fft_size/2;
low_index = round((low_freq*2/sr)*all_size)+1
low_freq = sr*(low_index-1)/(2*all_size)
high_index = round((high_freq*2/sr)*all_size)+1
high_freq = sr*(high_index-1)/(2*all_size)
up_index = round((high_freq*2/sr)*all_size)+1

if up_index > all_size
   disp(' Using',sr/2,'as high frequency')
   up_index = all_size
end

if low_index < 1
   disp(' Using DC as low frequency')
   low_index = 1
end

m = up_index - low_index + 1;

% Allocate memory
X = zeros(m,m);
polar_spec = zeros(m,2*m-1);
spec = zeros(m,m);
Indx = zeros(2*m-1,m);
```

```
% Generate phasors corresponding to each coordinate
Xr = kron((low_index-1:low_index+m-2),ones(m,1));
Xi = kron((low_index-1:low_index+m-2)',ones(1,m));
X = Xr + i*Xi;
Ang = angle(X);
spec_size = round(1+all_size-all_size/tan(Ang(m,1)))-1;
clear X Xr Xi

% Determine indexes corresponding to each polar coordinate
for kk=1:spec_size,
   angl = atan(all_size/(all_size-kk+1));
   [Y,I] = min(abs(Ang - angl*ones(m,m)));
   Indx(kk,1:m) = I(1:m);
end

for kk=1:spec_size-1,
   angl = atan((all_size-kk)/all_size);
   [Y,I] = min(abs(Ang - angl*ones(m,m)));
   Indx(kk+spec_size,1:m) = I(1:m);
end

function [spec]' = bispec(Indx,spec_size,chan1_spec,chan2_spec,low_freq,...
high_freq,sr,L)
% Function bispec_indx
%       [SPEC] = BISPEC(INDX,SPEC_SIZE,CHAN1_SPEC,CHAN2_SPEC,LOW_FREQ,...
%                              HIGH_FREQ,SR,L)
%       Computes the 2D spectral coherence function of two time series by
%       employing spectral smoothing using a rectangular window.
%       The algorithm first maps the raw spectrum from rectangular
%       coordinates to polar coordinates.  It then spectrally smooths the
%       raw spectrum using a 2D-convolution with the rectangular window.
%       It then maps the smoothed spectrum back to rectangular coordinates.
%       INDX and SPEC_SIZE must have been generated using MAKE_INDEX.
%
% Variables
%       INDX: Mapping matrix
%       SPEC_SIZE: Used to determine number of unique slopes
%       CHAN1_SPEC: DFT of first channel
%       CHAN2_SPEC: DFT of second channel
%       LOW_FREQ: Lowest frequency in spectral coherence plane
%       HIGH_FREQ: Highest frequency in spectral coherence plane
%       SR: Sample rate
%       L: Length of smoothing window
%
%       SPEC: Cross spectral coherence function
% Author: M. Reuter 9-5-95

% Set parameters and do sanity check
if low_freq >= high_freq
   disp(' ERROR: Requested low frequency is greater than the high frequency')
   return
end

chan1_spec = chan1_spec(:);
chan2_spec = chan2_spec(:);
all_size = size(chan1_spec,1)/2;
```

```
low_index = round((low_freq*2/sr)*all_size)+1
low_freq = sr*(low_index-1)/(2*all_size)
high_index = round((high_freq*2/sr)*all_size)+1
high_freq = sr*(high_index-1)/(2*all_size)
up_index = round((high_freq*2/sr)*all_size)+1

if up_index > all_size+1
   disp(' Using',sr/2,'as high frequency')
   up_index = all_size
end

if low_index < 1
   disp(' Using DC as low frequency')
   low_index = 1
end

m = up_index - low_index + 1;
%L = round(0.020*all_size)

% Allocate memory
X = zeros(m,m);
polar_spec = zeros(m,2*m-1);
spec = zeros(m,m);
raw_spec = chan1_spec(low_index:up_index)*chan2_spec(low_index:up_index)';

%Map to polar
for kk=1:2*spec_size-1,
   for ll=1:m
      polar_spec(ll,kk) = raw_spec(ll,Indx(kk,ll));
   end
end

% Spectral smoothing using the rectangular window.
polar_spec = conv2( polar_spec , ones(L,1), 'same' );

%polar_spec = conv2( polar_spec , ones(L,3), 'same' );

%Map to rectangular
for kk=1:2*spec_size-1,
   for ll=1:m
      spec(ll,Indx(kk,ll)) = polar_spec(ll,kk);
   end
end

%Normalize by PSDs
rpsd = diag(chan1_spec(low_index:up_index)*chan1_spec(low_index:up_index)');
Psd1 = conv2(rpsd, ones(L,1), 'same');
rpsd = diag(chan2_spec(low_index:up_index)*chan2_spec(low_index:up_index)');
Psd2 = conv2(rpsd, ones(L,1), 'same');
spec = spec./(sqrt(Psd1*Psd2'));
```

REPORT DOCUMENTATION PAGE

Form Approved
OMB No. 0704-0188

1. AGENCY USE ONLY *(Leave blank)*	2. REPORT DATE	3. REPORT TYPE AND DATES COVERED
	February 1996	Final: February 1996

4. TITLE AND SUBTITLE

SPECTRAL CORRELATION PROPERTIES OF TIME SERIES DUE TO AN ACOUSTIC SOURCE MOVING THROUGH AN OCEANIC WAVEGUIDE

5. FUNDING NUMBERS

PE: 0602435N
AN: DN304159
WU: SUBU

6. AUTHOR(S)

M. Reuter

7. PERFORMING ORGANIZATION NAME(S) AND ADDRESS(ES)

Naval Command, Control and Ocean Surveillance Center (NCCOSC)
RDT&E Division
San Diego, California 92152–5000

8. PERFORMING ORGANIZATION REPORT NUMBER

TD 2892

9. SPONSORING/MONITORING AGENCY NAME(S) AND ADDRESS(ES)

Office of Naval Research
800 N. Quincy Street
Arlington, VA 22217–5000

10. SPONSORING/MONITORING AGENCY REPORT NUMBER

11. SUPPLEMENTARY NOTES

12a. DISTRIBUTION/AVAILABILITY STATEMENT

Approved for public release; distribution is unlimited.

12b. DISTRIBUTION CODE

13. ABSTRACT *(Maximum 200 words)*

The time series representing the acoustic energy received at two sensors due to a source moving through an oceanic waveguide can exhibit strong spectral correlation between different frequencies. This correlation can be exploited to enhance passive detection of moving targets—particularly in shallow-water and near-field environments.

The structure of this spectral correlation is derived in this document. It is also shown that established techniques can estimate the spectral correlation from time series. This algorithm is assessed on real underwater acoustic data. Excellent agreement is observed with theory.

14. SUBJECT TERMS

Mission Area: Ocean Surveillance

two-dimensional spectral coherence
signal and array processing
acoustic surveillance

15. NUMBER OF PAGES

16. PRICE CODE

17. SECURITY CLASSIFICATION OF REPORT	18. SECURITY CLASSIFICATION OF THIS PAGE	19. SECURITY CLASSIFICATION OF ABSTRACT	20. LIMITATION OF ABSTRACT
UNCLASSIFIED	UNCLASSIFIED	UNCLASSIFIED	SAME AS REPORT